ANL/MCS-TM-384

Argonne NATIONAL LABORATORY

Nek5000 Enhancements for Faster Running Analysis

Mathematics and Computer Science

ANL/MCS-TM-384

Nek5000 Enhancements for Faster Running Analysis

prepared by

Misun Min[1], Ananias Tomboulides[1], Paul Fischer[1], Elia Merzari[2], Dillon Shaver[2], Javier Martinez[2], Haomin Yuan[2], and YuHsiang Lan[1]

[1] Mathematics and Computer Science Division, Argonne National Laboratory
[2] Nuclear Science and Engineering Division, Argonne National Laboratory

September 27, 2019

Contents

Executive Summary

The goal of this milestone is to enhance the performance of Nek5000 for thermal-hydraulics analysis.

In this milestone, the focus is on accelerating the time to solution for the coupled calculations of turbulent flows and thermal variations having different time scales that which require resolution of fine-scale structures. The main artifacts delivered include the following:

- Developing steady-state solvers for rod bundles and pebble beds
- Enhancing RANS solvers with improved stability and performance

This document covers work primarily funded under the NEAMS program. We note that the achievements listed here would have been impossible without a strong collaboration between the NEAMS team and ECP-CEED team. This synergy was enabled by algorithmic developments funded by DOE ECP Co-Design CEED and DOE ASCR Applied Math program.

In this document we are reporting some details on the algorithmic strategies and their results.

1 Introduction

The goal of this milestone is to enhance the performance of Nek5000 for thermal-hydraulics analysis. In order to achieve the milestone, a strong collaboration between NSE/NEAMS and MCS/ECP-CEED's Nek5000 development teams was essential, which was brought by synergistic efforts between NEAMS, CEED and ECP application collaborations.

For the thermal-hydraulics analysis, hundreds of thousands of flow channels comprise turbulent flow with very fine solution scales. The channels are typically hundreds of hydraulic diameters in length. While the turbulence is challenging to resolve, it tends to reach a statistically fully-developed state within just a few channel diameters, whereas thermal variations take place over the full core size. This poses a challenge for coupled calculations. It is unpractical and too expensive to consider performing a full LES calculations throughout the whole core. Acceleration that couples the solution through the use of steady-state solvers is necessary.

In this milestone, the focus is on accelerating the time to solution for the coupled calculations of turbulent flows and thermal variations at different time scales that have challenging fine scale spatial requirements. In this document we report some details on the algorithmic developments and their performance that include the following:

- Developing steady state solvers for rod bundles and pebble beds
- Enhancing Reynolds-averaged Navier-Stokes (RANS) solvers with improved stability and performance

For the thermal transport, steady-state solvers employ fast-diagonalization-based preconditioners that are based on low-rank-tensor approximations to the governing spectral element operators [1, 2]. These preconditioners are embedded in an outer Jacobian-Free Newton Krylov (JFNK) method [3]. For the RANS transport, stability-enhanced k-ω and k-τ models are considered.

2 Steady Thermal Solvers

Rod bundles represent an essential component of both classical and modern nuclear power plants. In most concepts, fuel assemblies comprise a large number of packed cylinder arrays of rods containing the nuclear fuel and surrounded by the liquid coolant. The prediction of the temperature distribution within the rod bundle is of major importance in the reactor design and is determined primarily by the flow characteristics in the subchannels bounded by adjacent rods. The problem lies, however, in the high Reynolds number that characterizes these flows, which dictates the required local resolution and also an increment in the timescale separation. This leads to smaller timesteps and longer transients, eventually making these simulations infeasible.

In collaboration with NEAMS and CEED's Nek5000 teams, we explored overcoming the excessive cost of large eddy simulations (LES) of full-length heated rod bundle calculations. Nek5000's steady-state solvers, developed under the ECP CEED project, have been applied for solving steady thermal flows for a long rod bundle and pebble beds geometries. We demonstrate an improved performance for a rod bundle [4] and preliminary results for pebble bed simulations. We also describe the algorithmic approaches that are based on Schwarz preconditioned fast diagonalization

methods [1, 2] and Jacobian-Free Newton Krylov methods [3]. Some of the efforts have been published, and the others are currently in preparation for journal publications.

2.1 LES-Based Turbulent Thermal Stress Models for Rod Bundle Simulations

While LES of an entire rod bundle is prohibitively expensive in most cases, the simulation of a small axial section of a bare rod is typically affordable. the NEAMS team's strategy is to use average and fluctuating information from a "small" but highly resolved LES of a single rod to build custom models of the turbulent thermal stresses that can be employed in the simulation of the entire full-length rod (see Figure 1). The idea reported here consists of using the information from the small LES calculation to determine the appropriate turbulence viscosity or turbulent thermal diffusivity that could be used to solve only for the temperature field in a pseudo-RANS approach. The detailed work has been published in IJHMT [4]; this report focuses on its subset, namely, the results by Nek5000's steady-state solver.

While the fluid viscosity does not depend on temperature under a valid assumption for the cases that are considered for the proposed methodology, velocity equations are completely unlinked to the temperature field. Using the Reynolds-averaging operator, one may divide instantaneous fields in an average part (time average for statistically steady flows) and a fluctuating part (i.e., $u_i = \bar{u}_i + u_i'$). When this approach is applied to the Navier-Stokes equations, the RANS equations are obtained as

$$\frac{\partial \overline{u}_i}{\partial t} + \frac{\partial}{\partial x_j}\left(\overline{u}_i \overline{u}_j\right) = -\frac{1}{\rho}\frac{\partial \overline{p}}{\partial x_i} + \frac{\partial}{\partial x_j}\left[\nu\left(\frac{\partial \overline{u}_i}{\partial x_j} + \frac{\partial \overline{u}_j}{\partial x_i}\right)\right] + \frac{\partial}{\partial x_j}\left(-\overline{u_i' u_j'}\right), \tag{1}$$

$$\frac{\partial \overline{u}_i}{\partial x_i} = 0, \tag{2}$$

$$\frac{\partial \overline{T}}{\partial t} + \overline{u}_j \frac{\partial \overline{T}}{\partial x_j} = \frac{\partial}{\partial x_j}\left(\alpha \frac{\partial \overline{T}}{\partial x_j}\right) + \frac{\partial}{\partial x_j}\left(-\overline{u_j' T'}\right), \tag{3}$$

where the turbulent heat fluxes can be modeled following a gradient diffusion hypothesis,

$$-\overline{u_j' T'} = \alpha_t \frac{\partial \overline{T}}{\partial x_j}. \tag{4}$$

Considering the proposed methodology, once the average velocity field and the turbulent diffusivity are obtained by the pseudo-RANS approach, one may solve for the Reynolds-averaged

Table 1: CPU time and number of iterations required to reach L_2 errors at the level of 10^{-7}, using 8 KNL nodes (512 MPI ranks) on Argonne's Bebop cluster.

Case	No. of Iterations			CPU Time (min)		
tol	10^{-2}	10^{-4}	10^{-6}	10^{-2}	10^{-4}	10^{-6}
BDF1/EXT	75275	34456	23026	154	97	114
BDF2/EXT	63854	31854	22371	130	90	106
BDF3/EXT	57163	30063	22095	117	85	103
SS	60			12		

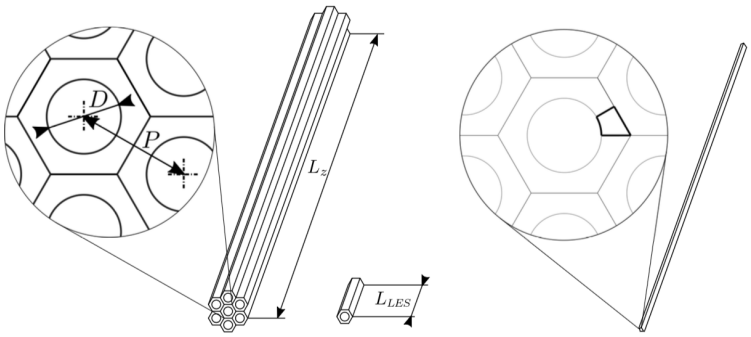

Figure 1: Geometry for bare rod in triangular array [4]. L_{LES} represents the length used for the pseudo-RANS approach, which is shorter than the full length L_z.

temperature field by considering the transient problem as described in Eq. (3), until a steady state is reached. Standard transient solvers in Nek5000 would need to advect the solution over times $\tau \gg \Delta t$, where Δt is the step size, limited by stability. An alternative approach for accelerating the convergence of the thermal advection is to consider a steady-state solver. In this framework, the equation to be solved by the steady-state solver is

$$\overline{u}_j \frac{\partial \overline{T}}{\partial x_j} = \frac{\partial}{\partial x_j}\left((\alpha + \alpha_t)\frac{\partial \overline{T}}{\partial x_j}\right), \tag{5}$$

where $\overline{u}_j$, α, and α_t are given. We demonstrate the performances of the steady-state (SS) solver and the transient solvers. In particular, the solution of the temperature field with the pseudo-RANS approach was obtained based on the kth-order time discretization schemes involving the BDFk with extrapolations (EXT). The temperature field was initialized to T_0 in the entire domain. To obtain a reference solution, we ran the SS solver until full convergence (machine precision) to produce a steady solution $\overline{T}_{ref}$. In the subsequent simulations, $\overline{T}_{ref}$ was taken as a reference, and the error of the predicted $\overline{T}$ with respect to $\overline{T}_{ref}$ was evaluated for each approach at each timestep in the L_2 norm.

For the transient solver, the timestep was fixed so that the maximum Courant number based on the frozen velocity field was $CFL = 0.5$. Three tolerances of the linear Helmholtz solver were chosen for the convergence criteria of each time step: $tol = 10^{-2}$, 10^{-4}, or 10^{-6}. For both the SS and BDFk/EXT schemes, the simulations were run until they reached the level of errors 10^{-7} in the L_2 norm. We calculated the evolution of the error norm, the required number of iterations, and the simulation time using 8 KNL nodes (512 MPI ranks) on Argonne's Bebop cluster. The results are shown in Figure 2 and listed in Table 1.

Figure 2 shows the convergence behaviors of the transient solution compared with the reference solution for the BDFk/EXT schemes. We observe a significant increase in the computational cost as the tolerance gets tighter with $tol = 10^{-6}$. The significant computational cost of increasing the convergence of each timestep (tightening the tolerance to $tol = 10^{-6}$) or increasing the order of accuracy can be clearly extracted from Figure 2 and Table 1. While slower at the beginning, the tighter tolerance in the linear solver might be worthwhile, however, since the required number of iterations to reach a given level of convergence might be reduced, as demonstrated in Figure 2. For

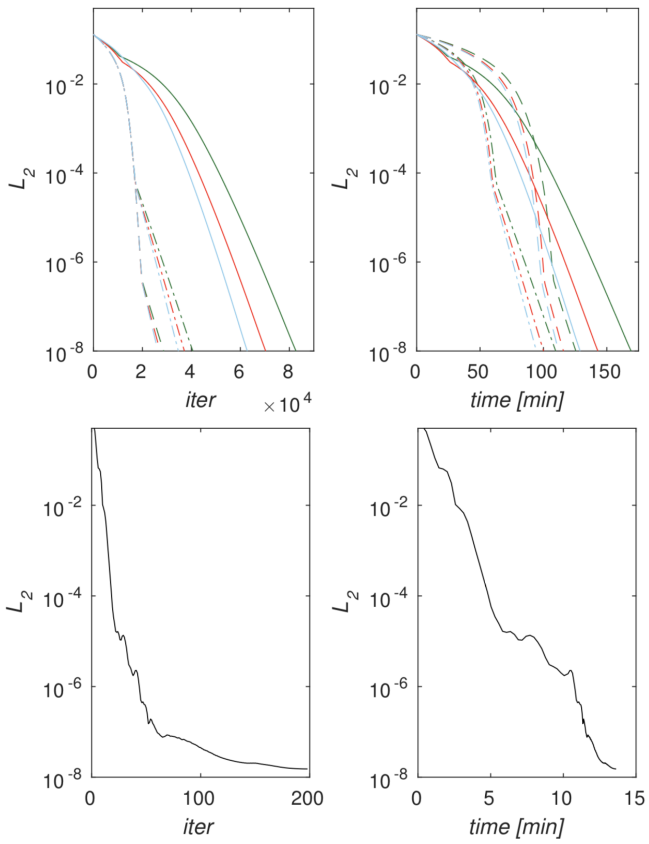

Figure 2: Error norm evolution for the transient solvers with BDF1/EXT (green), BDF2/EXT (red), BDF3/EXT (blue), and the SS solver (black). Transient solver results are shown for the linear solver tolerances of 10^{-2} (—), 10^{-4} (- · -), and 10^{-6} (- - -) with the timestep iterations and simulation time. The steady-state (SS) solver results are shown with the GMRES iterations and simulation time using $E = 21660$ spectral elements with $N = 7$ [4].

the simulations performed, considering the fastest time discretization scheme and larger tolerance (BDF3/EXT with $tol = 10^{-4}$), the SS solver is still about 7 times faster.

2.2 Pebble Beds

While the long rod bundle case solves the steady linear advection-diffusion equation (5) using GMRES with Schwarz-preconditioned fast diagonalization method, the JFNK method involving pseudo-timestepping is often considered relatively more stable for solving steady problems with very complex geometries. In this framework, the equation to be solved by the JFNK steady solver is

$$\frac{\partial \overline{T}}{\partial t} + \overline{u}_j \frac{\partial \overline{T}}{\partial x_j} = \frac{\partial}{\partial x_j}\left((\alpha + \alpha_t)\frac{\partial \overline{T}}{\partial x_j}\right). \tag{6}$$

Figure 3 demonstrates the steady thermal flows obtained by the Nek5000 JFNK solver while

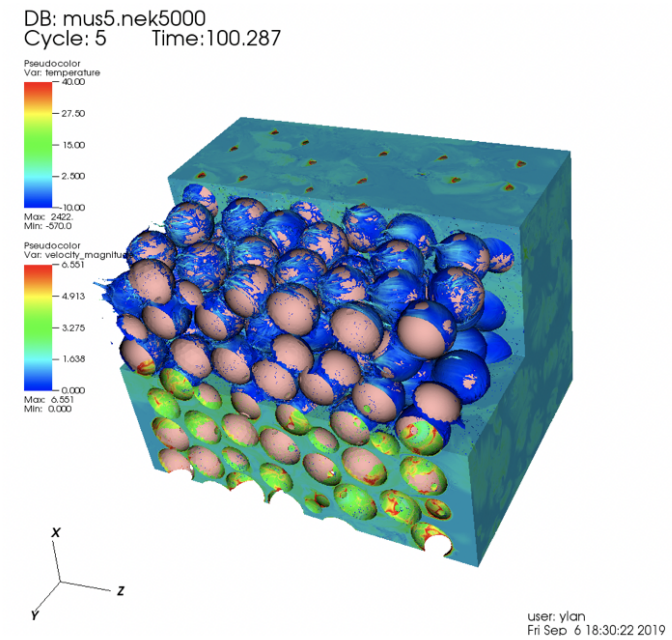

Figure 3: Temperature profile of pebble beds; 5-million spectral element mesh, representing 363 pebbles ($E = 5M, N = 5$); Steady-state solver based on JFNK method.

the velocity profile is given from precalculations. The geometry consists of 363 pebbles, simulated by 5 million spectral elements ($E = 5M$) with polynomial degree ($N = 5$). Our preliminary results show the JFNK is applicable to the complex geometry. The total pseudo-timestepping allows a very large timestep size (such as $\Delta\tau = 10^{12}$) from the initial pseudo-timestep and reaches to steady-state solution within 5 pseudo-timesteps. However it requires 10∼20 Newton iterations at each pseudo-timestep with large GMRES iteration counts. Adding preconditioning to JFNK is a necessary component to speed up the computation; this is currently work in progress.

2.3 Schwarz-Preconditioned Spectral Element Method for Steady Thermal Flow

Nek5000's steady-state solver uses a tensor product-based fast diagonalization method implemented for an overlapping Schwarz smoothing technique, integrated into a spectral element multigrid preconditioner [1, 2]. The tensor-product overlapping Schwarz spectral element multigrid preconditioner is formulated for the advection-diffusion operators based on spectral element discretizations and applied as a preconditioner for the GMRES procedure for solving Eq. (5).

The steady-state advection-diffusion and steady-state Navier-Stokes (NS) equations share a nonsymmetric, non-positive-definite character arising from advective transport. Preconditioning these systems for tensor-product-based spectral element methods presents unique challenges and opportunities. Following earlier work for the Poisson and Stokes problems [5, 6, 7, 8], we developed a p-multigrid (PMG) strategy that uses overlapping Schwarz solves for a smoother at each level. For

the steady advection-diffusion problem, PMG is used directly as a preconditioner within a Krylov subspace projection (KSP) method such as GMRES.

The smoother for our current p-multigrid preconditioner is based on a simple Richardson iteration involving a preconditioner, M. Coupling this with a coarse-grid correction leads to the two-level preconditioner given by the following pseudo-code.

$$\begin{aligned} &\textit{Approximate the solution to } L\underline{x} = \underline{b};\ \underline{x}_0 = 0\textit{:} && (7)\\ &\quad \underline{x}_1 = \underline{x}_0 + M(\underline{b} - L\underline{x}_0)\\ &\quad \underline{r}_1 = \underline{b} - L\underline{x}_1\\ &\quad \underline{r}_c = J_c^T \underline{r}_1\\ &\quad \underline{x}_c = L_c^{-1}\underline{r}_c && (8)\\ &\quad \underline{x} = J_c\underline{x}_c \ \text{(return } \underline{x}) \end{aligned}$$

Here, L is assumed to be the spectral element advection-diffusion operator, $M \approx L^{-1}$ is the Schwarz smoother, and $L_c = J_c^T L J_c$ is the coarse-grid system with J_c an interpolator from polynomial degree $p' < p$ to polynomial degree p within each spectral element. The coarse-grid problem (8) is solved by an invocation of the same two-level strategy, starting on a coarser grid, which leads to a classic p-multigrid, or by an iterative KSP scheme.

2.4 Jacobian-Free Newton Krylov Method for Steady Thermal Flow

Our JFNK method is introduced in [3] for solving drift-diffusion systems, coupled with a Poisson equation describing electric potential. This approach has been directly extended to Navier-Stokes and RANS models. In [3], we provide detailed studies of the choices of parameters that can assure accuracy and efficiency. Our spatial discretization is based on the spectral element method using curve-fitted hexahedral elements. We apply a backward difference formula to the semidiscrete form $\frac{d\underline{u}}{dt} = \underline{f}(\underline{u})$ and build a system of nonlinear equations $\underline{g}(\underline{u})$ expressed with the timestep size $\Delta\tau$ and $\underline{f}(\underline{u})$ during the pseudo time-transient process. Then we solve the resulting nonlinear system $\underline{g}(\underline{u}) = 0$ by the Newton method until the solution reaches steady state globally over time. The key ideas of the approach are how to compute the Jacobian matrix-vector product in Newton iterations and how to calculate the function $\underline{f}(\underline{u})$. We approximate the Jacobian metrix-vector product by finite differences and $\underline{f}(\underline{u})$ obtained by a backward difference formula using a local timestep Δt. With proper choices between $\Delta\tau$ and Δt, our method allows a larger pseudo-transient timestep size $\Delta\tau^n$ as the global time-integration evolves, and thus the total number of pseudo-transient timesteps can be significantly reduced to reach the steady solution.

3 Reynolds-Averaged Navier-Stokes Solvers

We investigated two approaches for the boundary layer treatment in our Nek5000 RANS solver: (1) the wall-resolved *regularized* approach [9] where we have to use adequate resolution inside the very thin log and viscous sublayers and (2) the new *wall-function* approach [10] where we do not need such high resolution as we move the boundary to a $y+$ of about 50–100. The wall function approach does not need to resolve the very sharp profiles immediately adjacent to the wall. Hence, the source

Table 2: Drag and lift coefficients (aoa=0). Experimental data: NASA-TM-4074 [11].

	Nek5000 results				References		Exper.
model	kw98 (N=7/N=11)	kτ98 (N=7)	kw06 (N=7/N=11)	kτ06 (N=7)	CFL3D	FUN3D	
drag	0.00872 / 0.00843	0.00842	0.00861/0.00833	0.00832	0.00854	0.00837	∼0.0081
lift	±1E-5/±1E-5	1.55E-5	±1E-5/±1E-5	1.21E-5	∼0	∼0	∼-0.01

Table 3: Drag and lift coefficients (aoa=10). Experimental data: NASA-TM-4074 [11].

	Nek5000 results				References		Exper.
model	kw98 (N=7)	kτ98 (N=7)	kw06 (N=11)	kτ06 (N=7/N=9)	CFL3D	FUN3D	
drag	-	0.01507	0.01391	0.01468/0.01432	0.01259	0.01297	∼ 0.012
lift	-	1.0582	1.0639	1.0592/1.0609	1.0958	1.1012	∼ 1.075

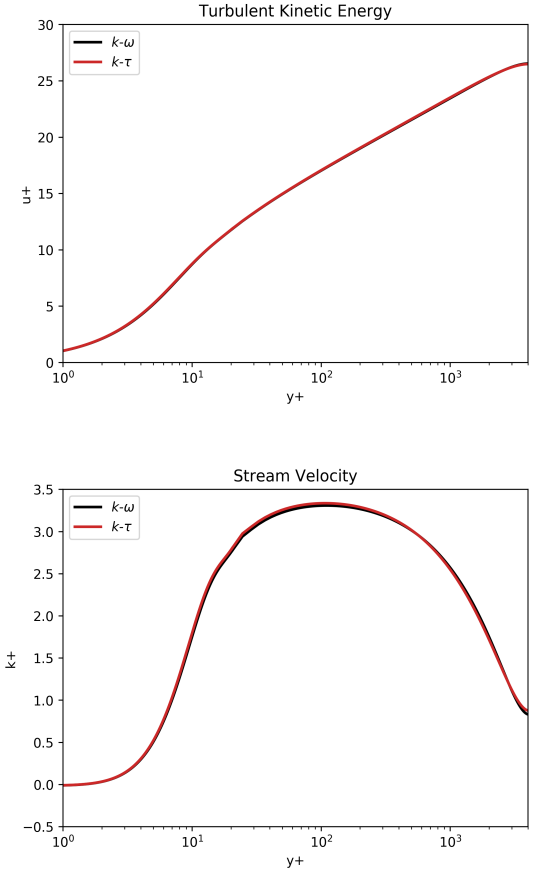

Figure 4: Comparison of mean streamwise velocity u^+ and turbulent kinetic energy k^+ profiles for $k-\omega$ and $k-\tau$ models.

terms in the ω equation, which are treated explicitly, are not as large in the wall function approach and create less of a stability problem.

Our RANS model is based on a regularized k-ω model, including the turbulent kinetic k and the specific dissipation rate ω in addition to the velocity field $\mathbf{v}$. The model describes the turbulent properties of incompressible flows with

$$k = \frac{\langle u'^2 \rangle + \langle v'^2 \rangle + \langle w'^2 \rangle}{2}, \tag{9}$$

where u', v', and w' are fluctuation component of velocity vector around the ensemble-averaged mean velocity vector $\mathbf{v} = (u, v, w)$ governed by

$$\frac{\partial(\rho \mathbf{v})}{\partial t} + \nabla \cdot (\rho \mathbf{v}\mathbf{v}) = -\nabla p + \nabla \cdot \left[(\mu + \mu_t) \left(\nabla \mathbf{v} + \nabla \mathbf{v}^T - \frac{2}{3} \nabla \cdot \mathbf{v} \right) \right], \tag{10}$$

$$\frac{\partial(\rho k)}{\partial t} + \nabla \cdot (\rho k \mathbf{v}) = \nabla \cdot \left[(\mu + \frac{\mu_t}{\sigma_k}) \nabla k \right] + P - \rho \beta^* k \omega, \tag{11}$$

$$\frac{\partial(\rho \omega)}{\partial t} + \nabla \cdot (\rho \omega \mathbf{v}) = \nabla \cdot \left[(\mu + \frac{\mu_t}{\sigma_\omega}) \nabla \omega) \right] + \gamma \frac{\omega}{k} P - \rho \beta \omega^2 + S_\omega, \tag{12}$$

where μ is the molecular viscosity and μ_t is the turbulent viscosity with the continuity equation for incompressible flow

$$\nabla \cdot \mathbf{v} = 0, \tag{13}$$

and where S_ω is the cross-diffusion term, which is nonzero only for the kw06. (We denote the Wilcox 1998 [12] and 2006 [13] versions as kw98 and kw06, respectively.) We have implemented and tested several RANS approaches in Nek5000, including the regularized $k - \omega$ model above, as well as some versions of the $k - \epsilon$ model and the $k - \tau$ model described below. We have tested these models in turbulent channel flow, flow past a backward-facing step, and external flows, such as flow past a wind turbine blade and the NACA0012 airfoil at 0 and 10 degrees angle of attack (aoa).

We found that the $k - \tau$ model gives exactly the same results with the $k - \omega$ and for this reason we investigated this model more extensively and plan to use it further to study more complex flows. The main advantages of the $k - \tau$ model are that it does not rely on the wall-distance function or its derivatives and the terms appearing in the right-hand-side of the model equations are bounded close to walls.

As described in the next subsections, we also investigated ways to increase the stability, accuracy and robustness of our RANS approaches in order to be able to use a larger timestep. For this reason we have treated some of the terms appearing in the right-hand-side of the model equations implicitly for stabiliztation, as explained below.

3.1 Stability-Enhanced Wall-Resolved Models: $k - \omega$

We investigated the performance of several limiters, commonly used in the RANS literature, for the production terms in the k and ω equations as well as for the eddy viscosity. Two versions of the $k - \omega$ model were evaluated that differ in the values of some of the model coefficients; in addition, the 2006 model includes a so-called cross-diffusion term S_ω.

We found that for external flows it is important to limit the value of eddy viscosity in the far field, which is typically not well resolved, in order to avoid abrupt variations in total viscosity.

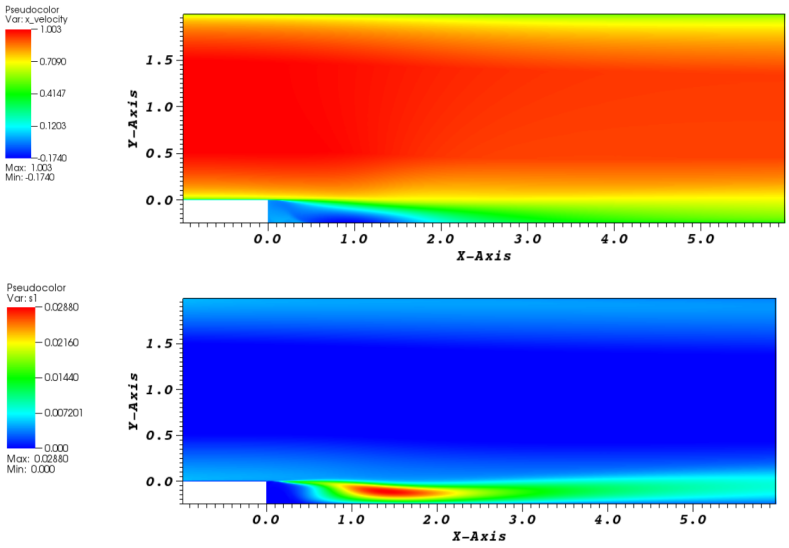

Figure 5: Comparison of mean streamwise velocity u^+ and turbulent kinetic energy k^+ profiles for the BFS at $Re = 149,700$ using the $k-\tau$ model of kw98.

Such variations can cause stability problems to the simulation and/or can significantly increase the number of pressure/velocity iterations needed for convergence at every timestep. The performance of the modified version of the $k-\omega$ model was tested for flow past a NACA0012 airfoil geometry, with varying free-stream conditions. With the modifications described above we obtained fully converted results for the drag and lift coefficients even for zero free-stream values of k.

Tables 2 and 3 show the values of the drag and lift coefficient obtained by using the two versions of the $k-\omega$ model (1998 and 2006) for flow past a NACA0012 airfoil at 0 and 10 degrees aoa. As can be observed, as resolution improves by increasing the polynomial order from $N = 7$ to $N = 11$ (8 and 12 points per direction, respectively), the model converges to the benchmark values of the drag and lift coefficients, which are also shown in the tables.

3.2 Stability-Enhanced Wall-Resolved Models: $k-\tau$

Another significant development during the past fiscal year was the implementation of the $k-\tau$ version of the $k-\omega$ model and the investigation of the scaling of all the terms appearing in the right-hand-side of the k and τ equations. The $k-\tau$ model was originally developed by Kalitzin et al. [14, 15] as an alternative implementation of the $k-\omega$ model. The equations for k and τ are derived from the $k-\omega$ equations by using the definition $\tau = 1/\omega$:

$$\frac{\partial(\rho k)}{\partial t} + \nabla\cdot(\rho k\mathbf{v}) = \nabla\cdot\left[(\mu + \frac{\mu_t}{\sigma_k})\nabla k\right] + P - \rho\beta^*\frac{k}{\tau}, \tag{14}$$

$$\frac{\partial(\rho \tau)}{\partial t} + \nabla\cdot(\rho \tau\mathbf{v}) = \nabla\cdot\left[(\mu + \frac{\mu_t}{\sigma_\omega})\nabla \tau\right] - \gamma\frac{\tau}{k}P + \rho\beta - 2\frac{\mu}{\tau}\left(\nabla\tau\cdot\nabla\tau\right), \tag{15}$$

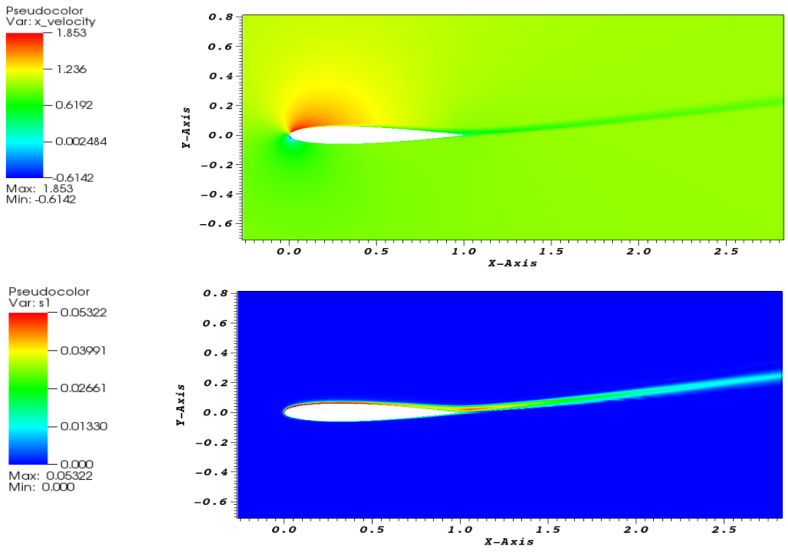

Figure 6: Comparison of mean streamwise velocity u^+ and turbulent kinetic energy k^+ profiles for the flow past a NACA0012 airfoil at $Re = 6M$ and a 10degree angle of attack using the $k-\tau$ model of kw98.

where now $G_k = P$, $Y_k = \beta^* k/\tau$, $G_\tau = \gamma\tau P/k$, $Y_\tau = \beta$, and $S_\tau = 2\nu\left(\nabla\tau \cdot \nabla\tau\right)/\tau$. In contrast to the original form of the $k-\omega$ model, in which the ω equation contains terms that become singular close to wall boundaries, all terms in the right-hand side of the k and τ equations reach a finite limit at walls and do not need to be treated asymptotically; that is, they do not require regularization for numerical implementation. The last term in the τ equation was implemented in the form proposed by Kok and Spekreijse (2000) [16], the following:

$$S_\tau = 2\nu\left(\nabla\tau \cdot \nabla\tau\right)/\tau = 8\nu\left(\nabla\tau^{1/2} \cdot \nabla\tau^{1/2}\right). \tag{16}$$

Extensive verification tests of the $k-\tau$ model were performed for channel flow, flow past a backward facing step (BFS), and flow past the NACA0012 airfoil at aoa=0 and 10. Both versions of the model coefficients (kw98 and kw06) were implemented. Figure 4 shows the comparison of the regularized $k-\omega$ and the $k-\tau$ model for flow in a channel at $Re = 10,950$. As can be observed, the agreement of the two models is excellent for both the mean velocity and the kinetic energy. The flow past a BFS at $Re = 149,700$ (Driver et al. [17]) was simulated using the $k-\tau$ model, and results were compared with the results of the regularized $k-\omega$ model (published in [9]). Figure 5 shows isocontours of mean streamwise velocity u and the k at steady state. The length of the recirculation zone from the RANS simulation using the $k-\tau$ model with the kw98 coefficients is equal to $6.59H$ (where H is the step height) and was found to be in excellent agreement with the corresponding value obtained by using the regularized $k-\omega$ model ($6.58H$). The recirculation zone length for the kw06 version is equal to $6.53H$.

We also investigated the performance of the $k-\tau$ model and compared it with the regularized $k-\omega$ model results (described in the preceding subsection) for the benchmark case of flow past the NACA0012 airfoil at aoa=0 and 10, which is relevant for external flows. The values of the drag and

lift coefficients obtained with the $k-\tau$ model are also shown in Tables 2 and 3 for the two versions of the model using varying resolution at $Re = 6 \times 10^6$. As can be observed in these tables, the drag and lift coefficients are in very good agreement with both the regularized $k-\omega$ model results and with the benchmark values from the NASA LARC website. Figure 6 shows the Isocontours of the mean streamwise velocity u^+ and turbulent kinetic energy k^+ profiles at steady state for the case of $Re = 6 \times 10^6$ and aoa=10 and computed by using the $k-\tau$ model of kw98.

3.3 Implicit Treatment of Source Terms in the Model Equations

A major development toward improving the robustness and efficiency of RANS in Nek5000 was the treatment of some of the source terms in the k and ω and the k and τ equations implicitly by including them in the left hand side of the equations. The terms that were treated implicitly are the following: For the $k-\omega$ model (i) the dissipation term in the k equation (Y_k) and (ii) two terms in the right-hand side of the ω equation that become unbounded close to walls at the same rate and need to be grouped together. For the $k-\tau$ model these terms are (i) the dissipation term in the k equation (Y_k) and (ii) the last term in the τ equation, which can become a source of instability. Treating all these terms implicitly did not increase the computational cost per timestep but allowed a significant increase of the timestep, which is now limited only by the convective CFL condition.

3.4 Reduced Boundary Layer Resolution by Using Novel RANS Wall Functions

Another way to reduce resolution requirements close to wall boundary layers is to use wall functions based on the log law. We are investigating this approach for RANS and LES and will pursue it further in the near future.

4 Conclusions and Future Work

We developed steady-state solvers and new RANS models to enhance the performance of Nek5000 for analysis of thermal-hydraulics problems with widely-disparate time-scales. The main focus is the following: (i) developing steady state solvers and performing simulations for a rod bundle and pebble beds and (ii) enhancing RANS solvers with improved stability and performance.

Our preconditioning strategy for a steady-state solver is based on Schwarz preconditioning with fast diagonalization, which enabled us to achieve 7× speedup for a long rod bundle case [1, 2, 4]. Adding this preconditioner to JFNK remains as a future work, which will improve performance further. The current Nek5000 production unsteady RANS (k-ω and k-τ) approaches employ backward difference for the time derivative coupled with implicit treatment of diffusion and explicit treatment of advection, which limits the timestep size to $CFL \sim 0.5$, which is a convective restriction. There remains room for further improvement by using characteristics [18] or Jacobian-free Newton-Krylov (JFNK) methods [3, 19] to circumvent the CFL constraint. Further collaborations with the ECP-CEED team will be pursued in this area in the near future.

Acknowledgments

Argonne National Laboratory's work was supported by the U.S. Department of Energy, Office of Nuclear Energy, Nuclear Energy Advanced Modeling and Simulation (NEAMS), under contract DE-AC02-06CH11357. Some portion of this work is supported by the Exascale Computing Project (17-SC-20-SC), a collaborative effort of two U.S. Department of Energy organizations (Office of Science and the National Nuclear Security Administration) and also by the U.S. Department of Energy, Office of Science, Office of Advanced Scientific Computing Research and under Contract DE-AC02-06CH11357.

References

[1] P. Brubeck and P. Fischer. Fast diagonalization preconditioning for nonsymmetric spectral element problems. *ANL/MCS-P9200-0719*, 2019.

[2] P. Brubeck, K. Kaneko, Y.H. Lan, L. Lu, P. Fischer, and M. Min. Schwarz preconditioned spectral element methods for steady flow and heat transfer. *ANL/MCS-P9199-0719*, 2019.

[3] Ping-Hsuan Tsai, Yu-Hsiang Lan, Misun Min, and Paul Fischer. Jacobi-free Newton Krylov method for Poisson-Nernst-Planck equations. *to be submitted*, 2018.

[4] Javier Martinez, Yu-Hsiang Lan, Elia Merzari, and Misun Min. On the use of LES-based turbulent thermal-stress models for rod bundle simulations. *Internaltional Journal of Heat and Mass Transfer*, 142:118399, 2019.

[5] P.F. Fischer. An overlapping Schwarz method for spectral element solution of the incompressible Navier-Stokes equations. *J. Comput. Phys.*, 133:84–101, 1997.

[6] P.F. Fischer, N.I. Miller, and H.M. Tufo. An overlapping Schwarz method for spectral element simulation of three-dimensional incompressible flows. In P. Bjørstad and M. Luskin, editors, *Parallel Solution of Partial Differential Equations*, pages 158–180, Berlin, 2000. Springer.

[7] P.F. Fischer and J.W. Lottes. Hybrid Schwarz-multigrid methods for the spectral element method: Extensions to Navier-Stokes. In R. Kornhuber, R. Hoppe, J. Périaux, O. Pironneau, O. Widlund, and J. Xu, editors, *Domain Decomposition Methods in Science and Engineering Series*. Springer, Berlin, 2004.

[8] J. W. Lottes and P. F. Fischer. Hybrid multigrid/Schwarz algorithms for the spectral element method. *J. Sci. Comput.*, 24:45–78, 2005.

[9] A. Tomboulides, M. Aithal, P. Fischer, E. Merzari, A. Obabko, and D. Shaver. A novel numerical treatement of the near-wall regions in the k-ω class of the rans models. *International Journal of Heat and Fluid Flow*, 72:186–199, 2018.

[10] O Kuzman, S Mierka, and S Turek. On the implementation of the k-ω turbulence model in incompressible flow solvers based on a finite element discretisation. *International Journal of Computing Science and Mathematics archive*, 1:193–206, 2007.

[11] Charles L. Ladson. Effects of independent variation of mach and reynolds numbers on the low-speed aerodynamic characteristics of the naca 0012 airfoil section. Technical Report NASA-TM-4074, L-16472, NAS 1.15:4074, NASA Langley Research Center, Hampton, VA, United States, 1988.

[12] D.C. Wilcox. *Turbulence Modeling for CFD*. DCW Industries, La Canada, CA, 1998.

[13] D.C. Wilcox. Formulation of the k-ω turbulence model revisited. *AAIA Journal*, 46(11):2823–2838, 2008.

[14] G Kalitzin, A.R.B. Gould, and J.J Benton. Application of two-equation turbulence models in aircraft design. *AAIA*, 96:0327, 1996.

[15] Gorazd Medic, Jeremy A Templeton, and Georgi Kalitzin. A formulation for near-wall RANS/LES coupling. *International Journal of Engineering Science*, 44:1099–1112, 2006.

[16] J.C. Kok and S.P. Spekreijse. Efficient and accurate implementation of the k-ω turbulence model in the NLR multi-block Navier-Stokes system. Technical Report NLR-TP-2000-144, National Aerospace Laboratory, 2000.

[17] S. Jovic and D.M. Driver. Backward-facing step measurements at low Reynolds number, Re=5000. Technical Report 108807, NASA Technical Memorandum, 1994.

[18] S. Patel, P. Fischer, M. Min, and A. Tomboulides. A characteristic-based, spectral element method for moving-domain problems. *Under Review*, 2018.

[19] Dana A Knoll and David E Keyes. Jacobian-free newton-krylov methods: a survey of approaches and applications. *Journal of Computational Physics*, 193(2):357–397, 2004.

Mathematics and Computer Science
Argonne National Laboratory
9700 South Cass Avenue, Bldg. 240
Lemont, IL 60439

www.anl.gov

Argonne National Laboratory is a U.S. Department of Energy laboratory managed by UChicago Argonne, LLC